



Nanomechanical behavior of coal with heterogeneous minerals and pores using nanoindentation

Baisheng Nie^{1,2} · Hengyi He^{1,2} · Peng Liu^{1,2} · Xianfeng Liu^{1,2} · Bozhi Deng^{1,2} · Yulong Zhao^{1,2} · Hao Zhang^{1,2} · Mingwei Cao³

Received: 8 December 2023 / Accepted: 12 March 2024 / Published online: 25 March 2024
© The Author(s), under exclusive licence to Springer-Verlag GmbH Germany, part of Springer Nature 2024

Abstract

The coal's mechanical properties have a significant influence on mining safety and the mine environment. Preparing a standard sample and conducting repeat mechanical testing are challenging because the coal is primarily soft, fragmented, and rich in developed fractures. This study used nanoindentation technology, combined with X-ray diffraction, small-angle X-ray, a high magnification microscope, and mechanical parameter scale-up analysis, to study the micromechanical of three coals being dominated by heterogeneous components and pores. The results show that load–displacement curves with different maximum loads (50 mN, 100 mN, and 200 mN) all appear the pop-in events, and coal heterogeneity affects the frequency of their occurrence. As the maximum load is increased, pop-in event of DSC appears once each, YW increases from zero to three times and HM decreases from four to two times. The heterogeneity of pore structure has little effect on residual displacement, which is mainly affected by hard minerals, and hard minerals reduce the law that residual displacement increases with the increase in maximum load. The micromechanical parameters of soft coals are mainly affected by large pores, while hard coals are mainly affected by hard minerals. The coal's heterogeneity does not affect the linear relationship between hardness and elastic modulus, but stronger heterogeneity will weaken the linear relationship between fracture toughness and elastic modulus. Compared to the mechanical parameters after scale-up, the values obtained based on nanoindentation are less than 15.588% larger, and the increase in the heterogeneity and hard minerals can make the predicted parameters more accurate. The nanoindentation technique can not only provide an efficient and accurate method for studying the mechanical properties of heterogeneous coal at the nanoscale, an important guide for large-scale coal.

Keywords Heterogeneous coal · Nanoindentation · Nanomechanics · Cross-scale

Introduction

Coal is a heterogeneous natural material composed of anisotropic minerals and multi-scale pores, with many internal mineral particles and delicate structures such as microcracks and micropores (Li et al. 2022a, b, c, d; Liu et al. 2022; Song et al. 2023; Xue et al. 2022). This results in different mechanical responses in terms of production safety (Le and Oh 2022; Ou et al. 2022; Wang et al. 2022), personnel health (Karacan et al. 2011; Qin et al. 2022; Wang et al. 2020; Zhong and Lin 2022), mine environment (Bhuiyan et al. 2021; Cao et al. 2023; Feng et al. 2020; Zhu et al. 2023), and contaminant leakage (Yang et al. 2020; Zhang et al. 2016; Zhang et al. 2022a, b), which affects personnel, equipment, and the working face environment (Li et al. 2023a, b). Therefore, understanding the microstructure and micromechanical properties of coal is essential for large-scale physical

Responsible Editor: Philippe Garrigues

✉ Peng Liu
rocliu@cqu.edu.cn

¹ State Key Laboratory of Coal Mine Disaster Dynamics and Control, Chongqing University, Chongqing 400044, China

² School of Resources and Safety Engineering, Chongqing University, Chongqing 400044, China

³ School of Emergency Management and Safety Engineering, China University of Mining and Technology (Beijing), Beijing 100083, China

experiments and a prerequisite for the safety of the mining industry (Chao et al. 2021; Yu et al. 2018).

At present, the commonly used micro-mechanical test methods include optical microscopy test (Kossovich et al. 2019a, b), scanning electron microscopy test (SEM) (Li et al. 2022a, b, c, d), high-resolution transmission electron microscopy (TEM) (Liu et al. 2023) and nanoindentation test (Phani et al. 2023), and depth-sensing nanoindentation (Epshtein et al. 2015). As an emerging technology, the nanoindentation test not only overcomes the disadvantages of the traditional uniaxial and triaxial test specimen size limitation and the difficulty of reuse but can also study the mechanical parameters of coal at a delicate level. Understanding and quantifying the mechanical properties of coals on micro- or nano-scale originating from the variability in their mineral and structural compositions play a vital role (Ma et al. 2020), thus revealing the process of coal yielding under load and providing new ideas and methods for studying micro- or nano-scale mechanical deterioration law of coal and damage destruction mechanism.

Nanoindentation has been used to measure the mechanical properties, including Young's modulus, hardness, fracture toughness, residual stress, and plastic work of different rocks (Kossovich et al. 2023; Li et al. 2022a, b, c, d; Manjunath and Jha 2019; Rózański et al. 2021; Shi et al. 2020). Sun et al. used nanoindentation averaging measurement method to characterize the micromechanical properties of coal, and the study showed that the hardness and elastic modulus decreased with increasing indenter load (Sun et al. 2020). Kossovich et al. analyzed the influence of organic components on the mechanical parameters of different coal ranks and investigated the elastic modulus and hardness of the specular and inert groups (Kossovich et al. 2019a, b). Zhao evaluated the creep behavior of tested sample using nanoindentation testing and found indentation size and loading strain rate influenced creep rate and the corresponding strain rate sensitivity (Zhao et al. 2018). Zhang et al. used optical microscopy to analyze the surface morphology of specially treated anthracite after indentation experiments (Zhang et al. 2022a, b). Liu et al. used a combination of nanoindentation tests, X-ray diffraction analysis, and field emission scanning imaging (FESEM-EDS) to analyze the modulus, hardness, and energy dissipation of three coals (Zhang et al. 2022a, b). Zhang et al. used SEM, micro-CT, and NMR to characterize the pore morphology of coal rocks and clarified that the highly heterogeneous spatial distribution of the indentation modulus is directly related to the morphology of the microstructure in coal (Zhang et al. 2018). However, the micromechanics do not suffice to provide a scientific reference for practical engineering applications, to connect microscopic and macroscopic mechanics; Mori–Tanaka homogenization methods are widely used (Li et al. 2022a, b, c, d). Xu et al. used the Mori–Tanaka method

to obtain rock macroscopic mechanical parameters from nanoindentation results (Xu et al. 2020). Li et al. studied nano-mechanical properties of shale by nanoindentation, and obtained the macro-scale values by Mori–Tanaka method (Li et al. 2022a, b, c, d). However, these studies are currently limited to the effects of heterogeneous mineral fractions and natural macroscopic cracks on the mechanical properties of the overall coals, focusing on the measurement and statistical analysis of mechanical parameters, limited to the level of phenomenological description and micro-mechanical characterization, and lacking the study of the controlling mechanisms of the evolution of mechanical properties.

This paper used X-ray diffraction (XRD) and small-angle X-ray scattering (SAXS) tests to quantify and classify the characteristics of coal fractions and micro-nanopores in different mining areas. Moreover, optical microscopy was used to qualitatively investigate the surface topography of coal, coal matrix, and micro-nanopores. Then, different maximum loads (50 mN, 100 mN, and 200 mN) were set to obtain the load–displacement curve and critical parameters of indentation tests (modulus of elasticity, hardness, fracture toughness), analyze the influence mechanism of mineral and pore heterogeneity on pop-in events in the curve, and discuss the reasons for the difference of micromechanical parameters of heterogeneous coals. Finally, homogenization theory is used to explore the cross-scale mechanical relationship and the control of microscopic heterogeneity on macroscopic mechanics. This study proposes a control mechanism for the minerals and pores of the micromechanical properties in heterogeneous coal.

Materials and methods

Samples collection and preparing

Three samples were collected from three coal mines (Dashucun coal mine, Yuwu coal mine, and Hami coal mine, see Fig. 1) and are numbered DSC, YW, and HM. DSC is on the western boundary of the Bohai Bay rift basin, with more tectonic development; YW is on the eastern flank of the Qingshui compound syncline basin, with a single developed tectonic structure; and HM is on the southern margin of the Hatu basin, with a complex tectonic structure. The samples were taken from different coal fields and different tectonic zones to ensure their heterogeneous characteristics (Cao et al. 2007; Cheng and Pan 2020; Tu et al. 2019).

The coals were immediately sealed in sealed bags after being taken out from the well and then sent to the laboratory for preparing powdered and block samples.

Powdered coal samples were used for XRD (Fig. 2a) and SAXS (Fig. 2b) testing: the coal briquettes were ground, screened (80 mesh and 200 mesh) and dried (80 °C, 12 h)

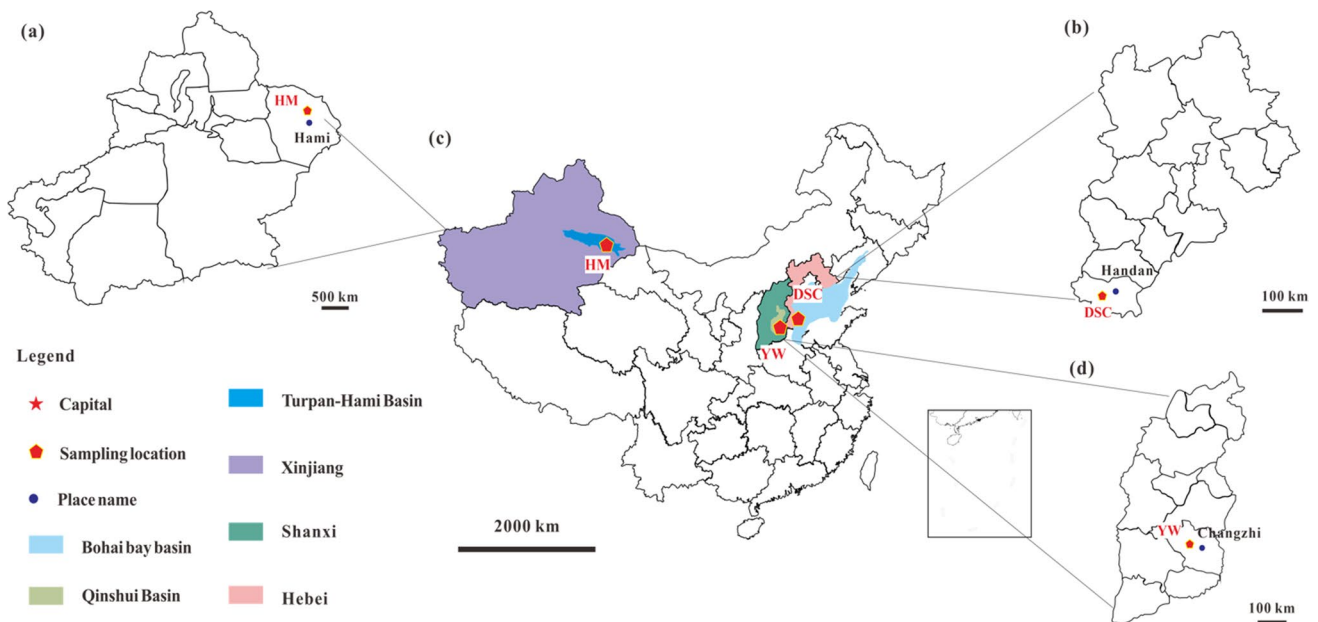


Fig. 1 Coal sample location and coal-bearing basin

to obtain uniformly dried coal dust particles. Coal powder of less than 200 mesh is used directly for XRD testing, while coal powder of less than 80 mesh is attached with 3 M adhesive tape to the hollow part in the center of the SAXS cuvette.

Block coal samples were used to nanoindentation (Fig. 2c). Firstly, the coals were made into block coal of 10 mm × 10 mm × 5 mm, and then polished and polished using a mechanical polishing platform, first rough polishing on one side, then fine polishing on the other side, to reduce the roughness of the nanoindentation surface, and at the same time to ensure that the samples were parallel to the top and bottom. For fine polishing, the coals were fixed on the polishing table with paraffin wax, and the test surfaces of the coals were polished sequentially with 320, 600, 1000, 2000, and 3000 grit sandpaper, and then, the coals were further polished sequentially with 5 μm and 0.05 μm polycrystalline diamond suspensions to obtain a finer surface. Finally, acetone and anhydrous ethanol were used to clean and wash the samples to ensure that the samples surface were clean, flat, and smooth, and the polished coals were placed in an oven at 80 °C for more than 12 h to ensure that the samples were thoroughly dried.

The study was carried out according to the following experimental procedure (Fig. 2.)

Coal mineral components and maceral analysis

They were analyzed by X-ray diffraction (XRD) and industrial analysis for mineral component determination, macerals (see Table 1), and coalification degree.

DSC and YW are high rank coals; HM is a medium rank coal with a wide variation in industrial analysis composition and heterogeneity of components. The mineral components of DSC and YW are dominated by amorphous organic matter and clay minerals, with small amounts of quartz and carbonate minerals, indicating that the matrix of DSC and YW is weak and low in strength; the mineral components of HM are dominated by carbonate minerals, amorphous organic matter, and quartz, with small amounts of clay minerals, indicating that the matrix of HM is better than that of DSC and YW, with high strength.

High magnification microscope analysis of coals surface

To understand the surface morphology, 3D scans of DSC, YW, and HM surfaces were carried out using a VHX-6000 high magnification microscope to obtain the surface morphology (see Fig. 3).

From Fig. 3 a, b, and c, the surface of DSC was rough, the pore structure was accompanied by fracture development, the structure was loose, many coal debris was distributed on the surface, and combined with the XRD results, most of the black material on the surface of the coal was amorphous organic matter. From Fig. 3 d, e, and f, the surface of YW was uneven, but without significant pore and fracture structure, many white grains and white filamentous streaks were distributed on the surface; the white minerals and white filamentous streaks may be carbonating minerals or clay minerals. From Fig. 3 g, h, and i, the surface of the HM was flat and smooth with few significant pores and microcrack

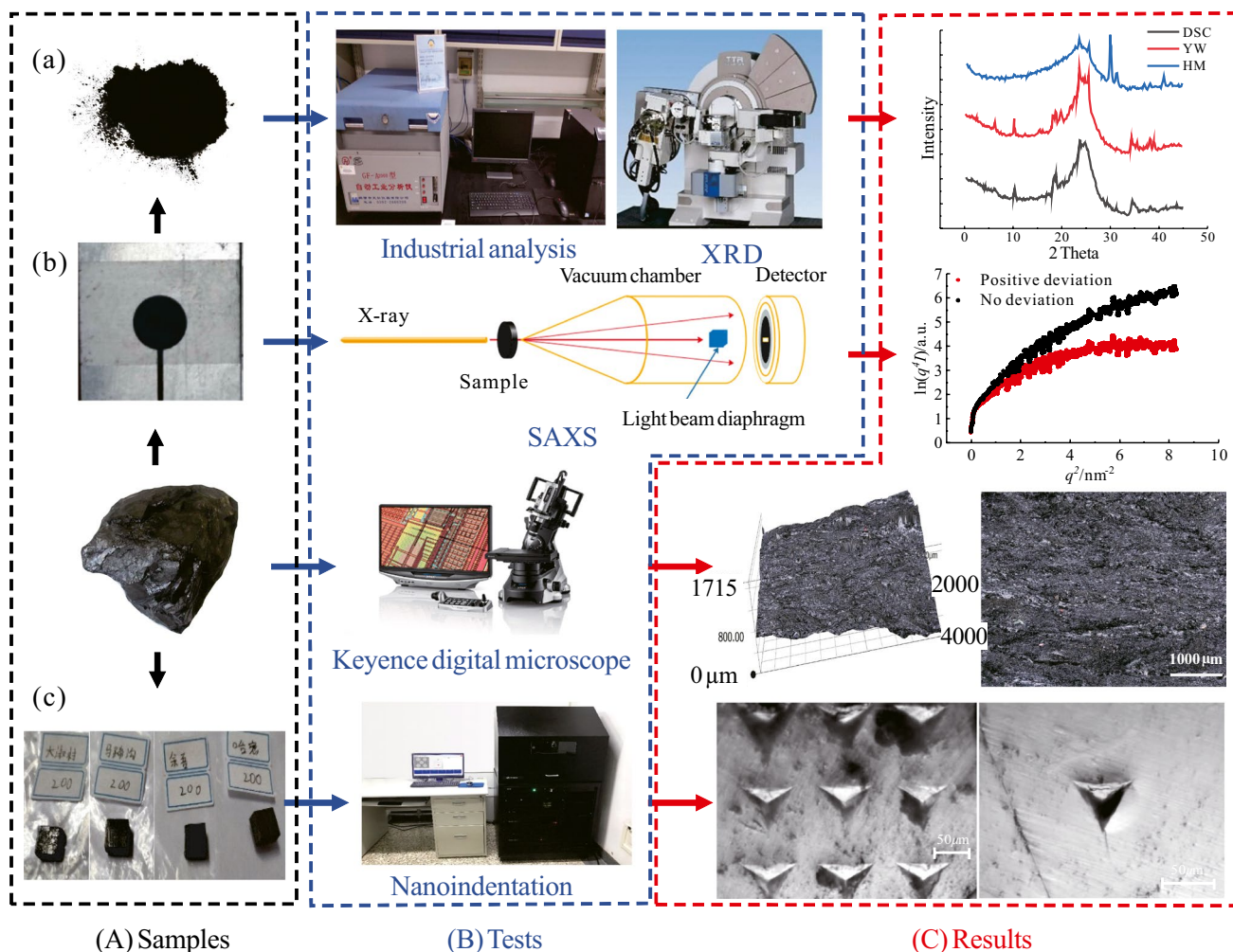


Fig. 2 Experimental schedule, where (a) powdered coal samples for XRD; (b) powdered coal samples for SAXS; (c) block coal samples for nanoindentation

Table 1 Mineral component and macerals

Sample	Quartz, %	Calcite, %	Non-crystal, %	Kaolinite, %	R_o , %	M_{ad} , %	A_{ad} , %	V_{daf} , %	F_{Cd} , %
DSC	4.53	2.67	77.73	15.07	2.32	1.03	15.47	12.43	73.26
YW	7.87	1.62	75.56	14.95	2.05	0.41	54.91	10.53	40.18
HM	15.55	42.59	32.42	9.24	0.94	2.03	2.92	33.15	63.58

structures. Many white minerals on the surface, the white minerals are quartz and carbonate minerals.

Small angle X-ray scattering analysis

The aperture, porosity, specific surface area, and surface fractal (it quantifies surface complexity surface complexity and heterogeneity; the upper and lower cutoff is $2 \leq D_s \leq 3$, and $D_s = 2$ for a smooth Euclidean geometric plane; $D_s = 3$ means that the surface is so complex that it fills up the space and becomes a solid) analysis were carried out for DSC, YW, and HM respectively (Fig. 4).

DSC has the largest average aperture, porosity, and specific surface area, respectively 17.92 nm, 9.81%, and 72.03 $m^2 \cdot g^{-1}$; it has the loosest structure; the minerals in the coal are pooled in the form of small particles; and its surface fractal dimension is the smallest ($D_s = 2.47$), with the most homogeneous structure of pores and minerals; YW has the intermediate aperture size but smallest porosity, 11.37 nm, 8.09%, and 50.18 $m^2 \cdot g^{-1}$, respectively, which has the smallest porosity but different pore sizes have variability, and the integrity of mineral particles is good, but due to its maximum surface fractal dimension is 2.75, it indicates that its pore and mineral structure distribution is the most

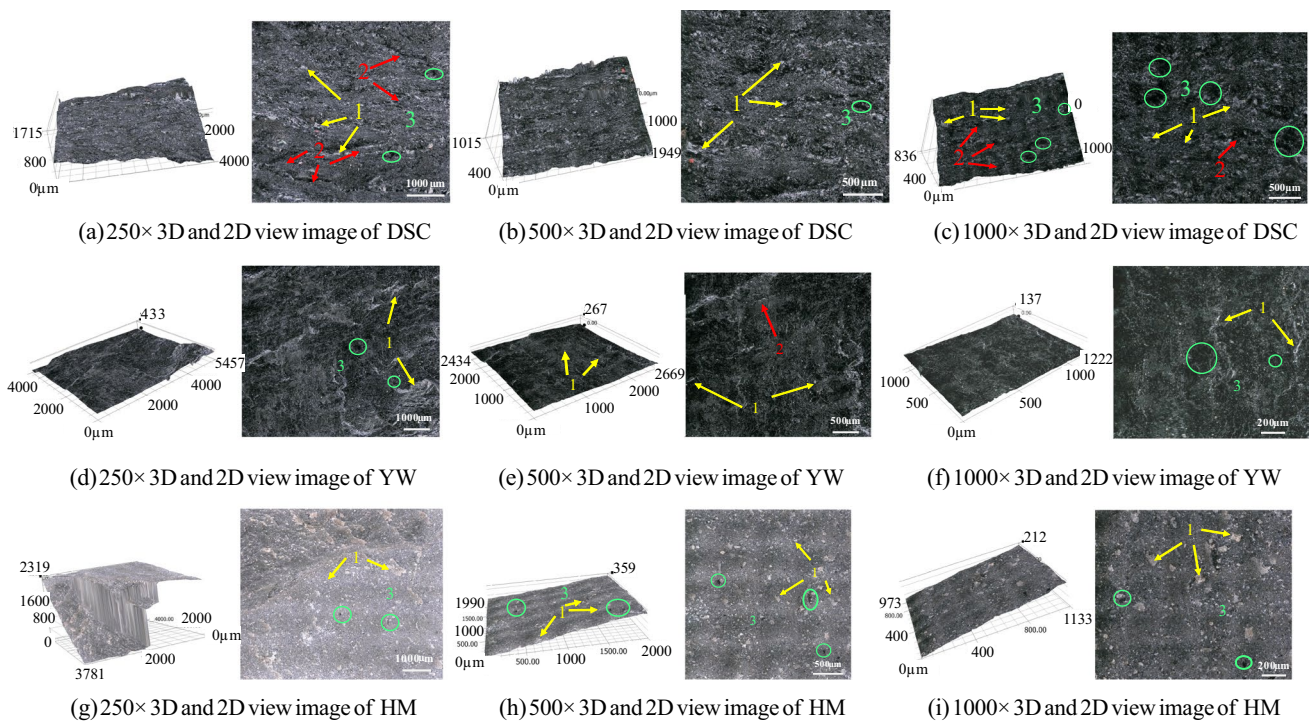


Fig. 3 Scanned image of coal samples, where (1) mineral phase; (2) fracture; (3) obvious hole

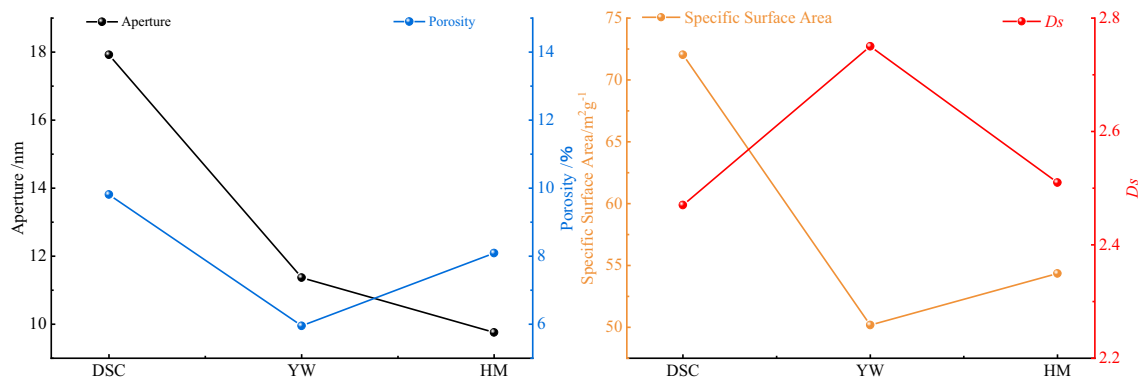


Fig. 4 Structure and surface fractal

anisotropic; combined with the scanning image, the HM have few significant pores and fractures in local area, but the parameters of the pores is affected by all pores and fracture on coal’s surface, which are very small compared to DSC and YW, thus causing the average aperture of HM to be the smallest, it is 9.76 nm, but the significant large pores cause the porosity and specific surface area not to be the smallest, which are 8.09% and 54.35 m²·g⁻¹, respectively, which indicates that the segmentation of the minerals by the pores is not significant, resulting in the high integrity of the minerals contained in the HM, and that its surface fractal dimension is smaller ($D_s = 2.51$), and its pores and mineral distribution is more homogeneous.

The heterogeneous mineral and pore structure of coals

To facilitate the exploration of the heterogeneity of the pore structures and mineral component, Three coals were simplified into a three-phase medium mechanical model (pore/fracture, coal matrix, and mineral phase) (Fig. 5) (Miller et al. 2008; Zhang et al. 2018), and the mineral phases could be classified into hard minerals (quartz-carbonate minerals) and soft minerals (amorphous minerals and clay minerals). Combined with the proportion of the components (Table 1) and the surface morphology (Fig. 3) analyses above, the physical models of the three coals were

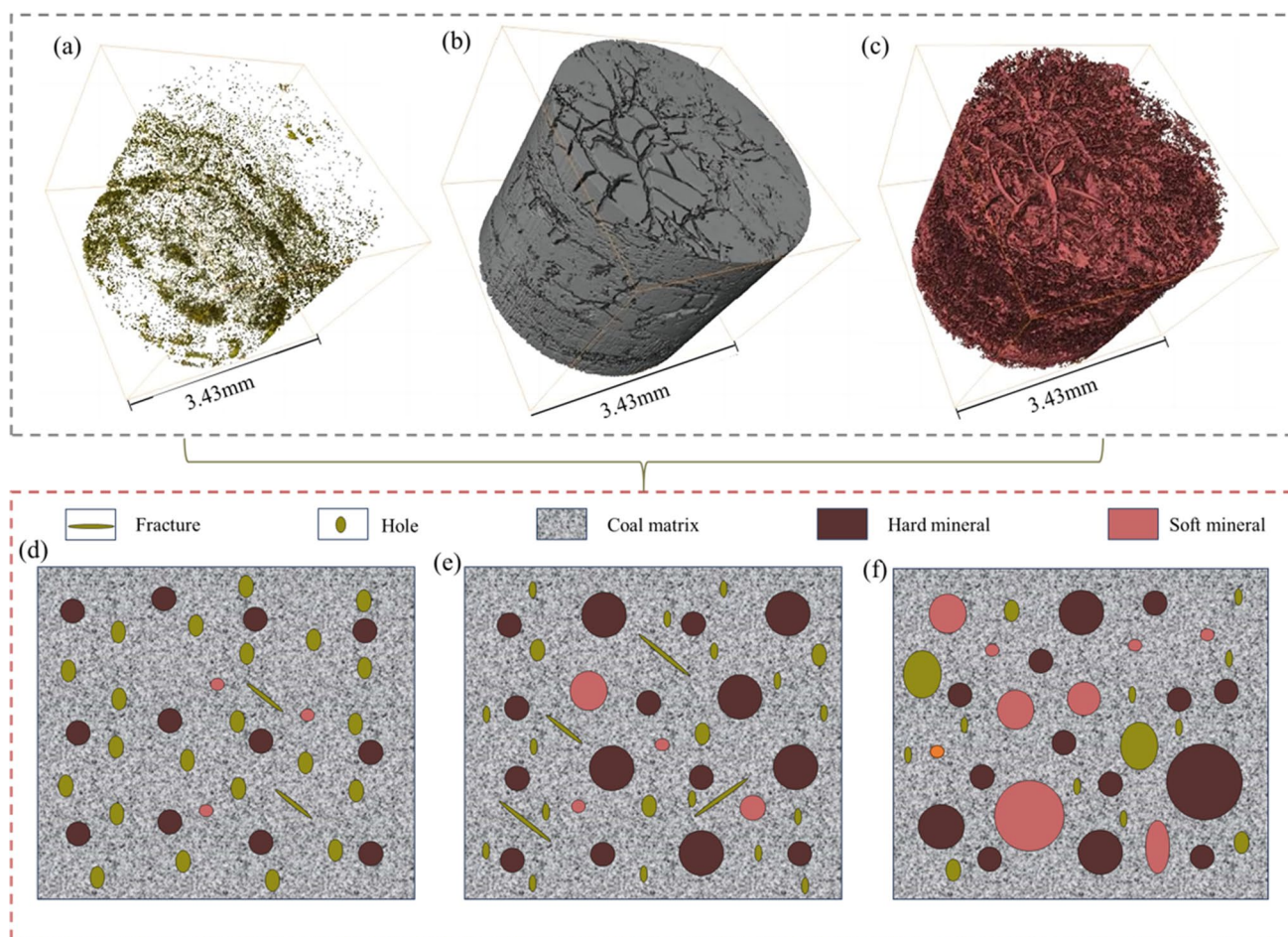


Fig. 5 3D visualization and physical models of coal: **a** voids/fractures; **b** coal matrix; **c** mineral phase; **d** DSC; **e** YW; **f** HM (Zhang et al. 2018)

established based on a three-phase medium mechanical model.

DSC has the loosest structure with uniformly spread pores, good uniformity of its aperture, fewer cracks, and weak physical properties of small mineral particles; YW has a more compact structure with significant cracks and weak physical properties of more uniform size and distribution of mineral particles; HM has the most compact structure but has significant large pore structure and non-uniformly distributed strength of hard minerals in large particles.

Nanoindentation experiment

Nanoindentation technique

The nanoindentation micromechanical testing is shown in Fig. 6 The Oliver-Pharr law is widely used to obtain the nanoindentation load–displacement curve (Borodich et al. 2015; Hu et al. 2015; Kossovich et al. 2019a, b; Li et al. 2023a, b; Oliver and Pharr 1992).

In Fig. 6, F_m is the maximum load applied during the nanoindentation experiment, mN; h_m is the peak displacement during the loading process, nm; h_c is the contact displacement when the maximum load is reached, nm; h_s is the maximum displacement of the sinking of the material surface during the load application process, nm; where $h_k = h_m - h_c$; h_k is the creep displacement during the holding phase, nm; h_p is the residual displacement during the unloading phase when the load is 0 mN; h_r is the tangential displacement of the load–displacement curve during the unloading phase, nm. In Fig. 6b, section A shows the loading phase of the nanoindentation experiment, section B shows the peak load retention phase, section C shows the unloading phase, the straight-line D is the tangent line of the initial phase of the unloading, and the slope S of the corresponding tangent line D is the contact stiffness. Three types of energy are generated during the unloading process: fracture energy (U_c), elastic energy (U_e), and plastic energy (U_p).

According to the Oliver-Pharr law, the load–displacement curve for the initial phase of unloading in the experiment can be described using the conventional power function.

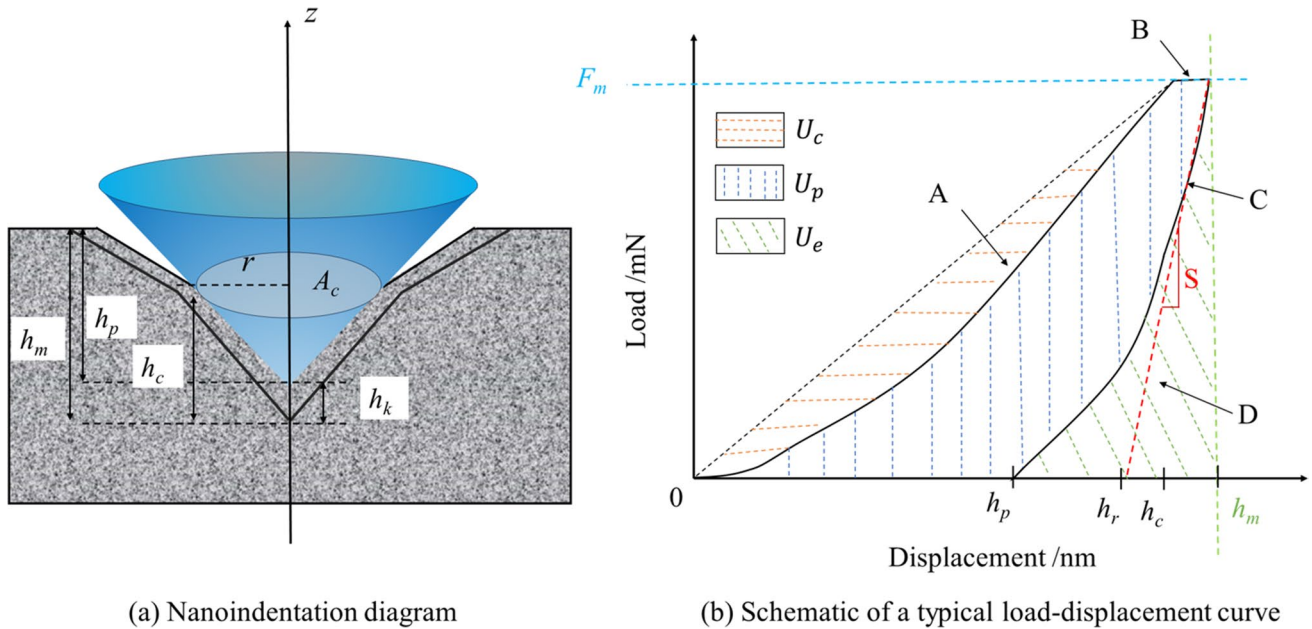


Fig. 6 Nanoindentation and typical nanoindentation curve

$$F_n = \alpha(h - h_p)^\beta \tag{1}$$

where F_n is the load, mN; α and β are constants derived by fitting the curve to the unloading phase; and h is the contact depth corresponding to F_n .

The contact stiffness of the sample can be obtained by deriving the power function fitted to the initial stage of unloading at the position of the maximum peak displacement.

$$S = \left(\frac{dF_n}{dh} \right)_{h=h_{max}} = \alpha\beta(h - h_p)^{\beta-1} \tag{2}$$

The contact depth h_c can then be obtained by using the following equation:

$$h_c = h_m - \varepsilon(h_m - h_r) \tag{3}$$

where ε is a constant related to the indenter. For Bose’s indenter, $\varepsilon = 0.7268$.

The relationship between the contact projection area (A_c) and the contact depth (h_c) of the indenter can be described by the following formula.

$$A_c = 24.5h_c^2 + C_1h_c^1 + C_2h_c^2 + \dots + C_8h_c^{28} \tag{4}$$

Since the indenter used in this paper is Berkovich indenter, the first term of Formula (4) can be used to describe the relationship between the contact projection area and the contact depth.

Therefore, the hardness (H_{IT}) and converted modulus (E_r) of the test sample can be calculated by the following formula.

$$H_{IT} = \frac{F_m}{A_c} \tag{5}$$

$$E_r = \frac{S\sqrt{\pi}}{2\eta\sqrt{A_c}} \tag{6}$$

where η is a constant, related to the indenter. For the Berkovich indenter (Bose indenter) used in this experiment, $\eta = 1.034$.

Since the stiffness of diamond indenter is extremely strong, the non-rigidity of diamond indenter has almost no influence on the test results. Therefore, in general, the converted modulus can replace the elastic modulus. When the influence of non-rigidity of the indenter is not ignored, the elastic modulus of the sample can be calculated by the following formula.

$$E_{IT} = \frac{1 - \nu_{IT}^2}{\frac{1}{E_r} - \frac{1 - \nu_i^2}{E_i}} \tag{7}$$

where E_{IT} and ν_{IT} , respectively, represent the microscopic elastic modulus and Poisson’s ratio of coal. Since Poisson’s ratio has little influence on the calculation of the above formula, $\nu_{IT} = 0.3$ is taken here. E_i and ν_i , respectively, represent

the elastic modulus and Poisson’s ratio of diamond indenters, $E_i = 1141$ GPa and $\nu_i = 0.07$.

According to Fig. 6b, total energy U_t generated during the whole nanoindentation experiment is the sum of fracture energy U_c , recoverable elastic energy U_e , and unrecoverable plastic energy U_p .

$$U_t = U_c + U_e + U_p \tag{8}$$

The sum of U_e and U_p can be obtained by the following formula.

$$U_e + U_p = \int_0^{h_m} F_n dh \tag{9}$$

$$U_t = \frac{F_m(h_m + h_k)}{2} \tag{10}$$

The critical energy release rate (G_c) is the ratio of U_c to the contact projection area (A_c).

$$G_c = \frac{\partial U_c}{\partial A_c} \tag{11}$$

Therefore, the fracture toughness (K_{Ic}) can be calculated by the following formula.

$$K_{Ic} = \sqrt{G_c E_r} \tag{12}$$

Nanoindentation scheme

The nanoindentation experiment scheme is as follows:

(a) Selection of areas with smooth surfaces and no obvious pore fracture for experiments (Fig. 7b).

(b) Preventing the load is too small cannot reflect the true mechanical properties of coal, at the same time consider avoiding the load is too large to produce a large number of cracks, so that the results of the error. The maximum load is set to 50 mN, 100 mN, and 200 mN, respectively, and the change rate of load during loading and unloading is constant, which is 0.4 mN/s, and the load is kept for 10 s after reaching the maximum load. Select a range of $200 \mu\text{m} \times 200 \mu\text{m}$ on the sample and press one point every $100 \mu\text{m}$ to form a 3×3 array with 9 points in total (Fig. 7c).

Results

Characteristics of the load–displacement curves

Three different maximum load nanoindentation experiments were carried out on heterogeneous coals. The load–displacement curves were obtained and plotted (Fig. 8). Under different maximum loads, load–displacement curves show an approximate trend. During the loading stage, displacement first increased rapidly and then slowly as the load increased. During the load holding stage, load remained constant,

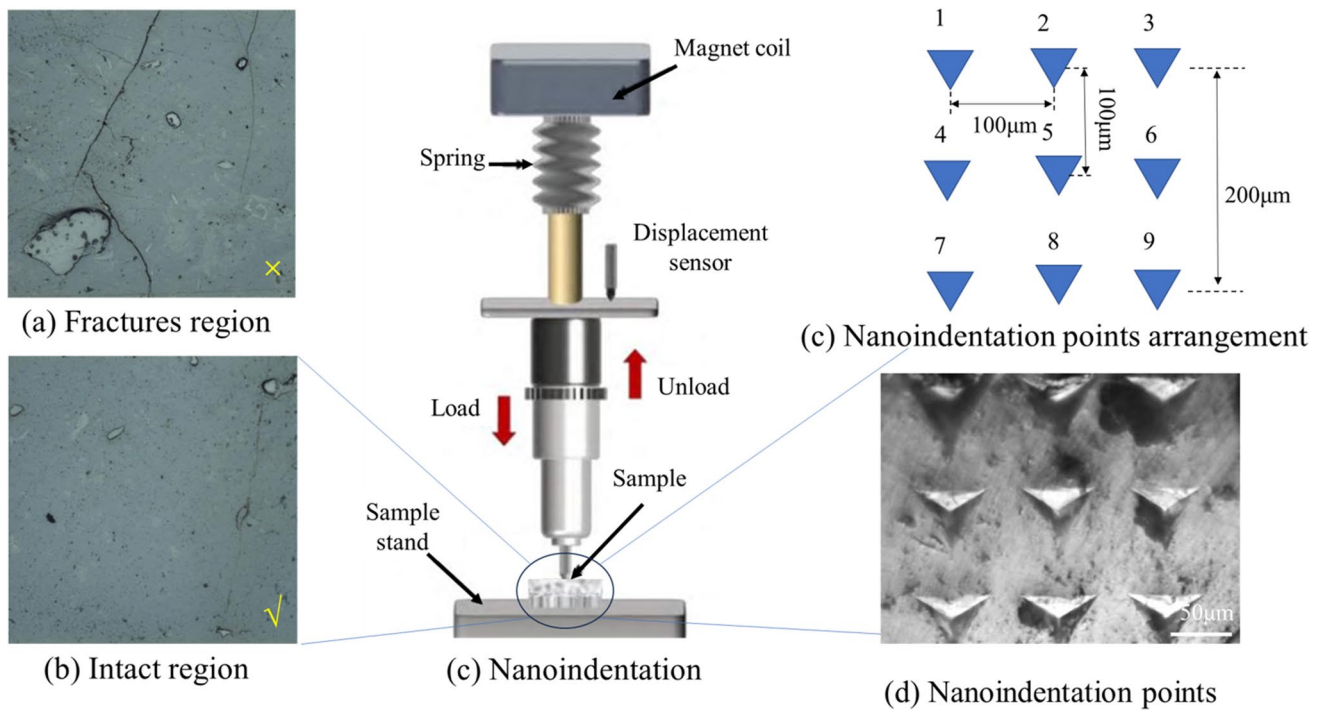


Fig. 7 Nanoindentation test

displacement increased, and creep deformation occurred on the surface of coals. After that, the unloading process begins, elastic deformation is recovered, and a certain amount of irrecoverable plastic deformation remains after unloading.

From Fig. 8 a, b, and c, the most homogeneous DSC appear one pop-in event under different maximum loads. With the increasing maximum load, the loads at which event occur show an increasing trend, respectively 11 mN, 67 mN, and 176 mN. At a maximum load of 50 mN, the pore structure with poor bearing capacity is the first to be damaged, and because it has the largest average aperture, it produces a pop-in event. At a maximum load of 100 mN, the pore and original fracture penetration occurs in a larger range of damage to produce a pop-in event. At a maximum load of 200 mN, the pore and fracture are compacted in the load process, destruction of minerals, under high pressure leading to a pop-in event.

Form Fig. 8 d, e, and f, more homogeneous YW with the increasing maximum load, pop-in event from zero times to three times. At a maximum load of 50 mN, small pores with low strength are first to destruct without a significant pop-in event. At a maximum load of 100 mN, the small pores are compacted, and the large pores and original fractures are successively destroyed to produce a large displacement so that there is a pop-in event. At a maximum load of 200 mN, the pop-in event increases significantly. The hard large pores to produce a displacement, and soft mineral rupture occurs with the displacement of the indenter, the large pores/fracture, and minerals again alternate destructive behaviors, which results in many pop-in events.

Form Fig. 8 g, h, and i, the most heterogeneous HM has pop-in events decrease from four times to two times with increasing maximum load; the heterogeneous characteristics cause the load–displacement curve to have a huge discrete

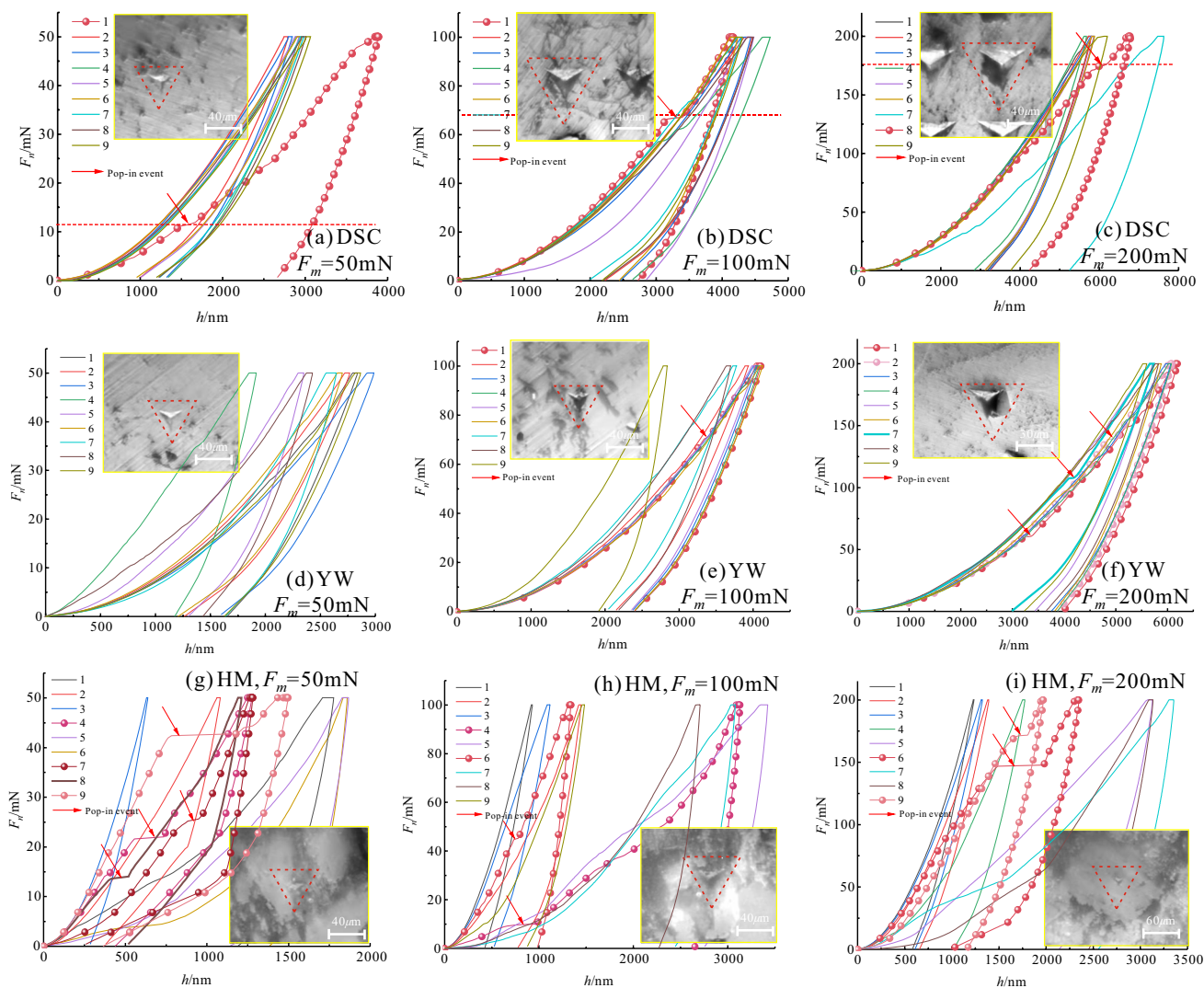


Fig. 8 The load–displacement curves of heterogeneous coals

shape and many pop-in events. At a maximum load of 50 mN, destruction of a large number of non-uniformly distributed macropores accompanied by compaction of small pores, which produces many displacement forming many pop-in events. At a maximum load of 100 mN, HM contain a large number of hard minerals that are not easy to damage, so the little soft minerals generate fewer pop-in events. At a maximum load of 200 mN, the hard minerals sudden slip cause the pop-in event under high load.

Nanoindentation load displacements become disordered as increasing homogeneity. Homogeneous coals develop from pore destruction, then fracture penetration, and finally mineral destruction, producing a similar number of pop-in events; more homogeneous coals experience small pores compact, then large pores destruction, and finally minerals undergoing destruction, producing a gradually increasing pop-in events; heterogeneous coals evolve from large pores undergoing destruction and compacting, then soft minerals undergoing destruction, and finally hard minerals slipping, producing a gradually decreasing pop-in events.

Characteristics of the load and displacement

From Fig. 9a, at maximum loads of 50 mN, 100 mN, and 200 mN, DSC average residual displacement was 1305.26 nm, 2412.67 nm, and 3547.53 nm; YW average residual displacement was 1429.58 nm, 2250.24 nm, and 3619.62 nm; HM

average residual displacement was 661.46 nm, 1521.53 nm, and 1341.26 nm. Coal is generally consistent with residual displacement increasing with maximum load, but strong heterogeneity alters this result.

DSC and YW mineral components are similar, but mineral size and pore size are different. Their residual displacement at different maximum loads are similar, indicating that the structural heterogeneity of components has little effect on the residual displacement. HM with strong heterogeneity at 50 to 100 mN corresponds to the larger residual displacements with increasing loads, while at 200 mN, this result changes. Because heterogeneous pores are compacted at low load and have little effect on the residual displacement, many heterogeneous hard minerals resist deformation and produce smaller displacements at high loads, resulting in reduced residual displacements.

Combined with nanoindentation image, at maximum load of 50 mN, YW have larger displacements due to the presence of large pores around indentation (Fig. 9f), while at maximum load of 100 mN, the indenter continues to penetrate deeper, and the damage zone does not expand to the adjacent primary fracture (Fig. 9g), while DSC has a large number of small grained minerals and a boundary fragmentation zone (Fig. 9d), resulting in a sudden increase in displacement over YW. At maximum load of 200 mN, YW crack conducts to surrounding pores and again generates a large damage (Fig. 9g), leaving the indenter center without a

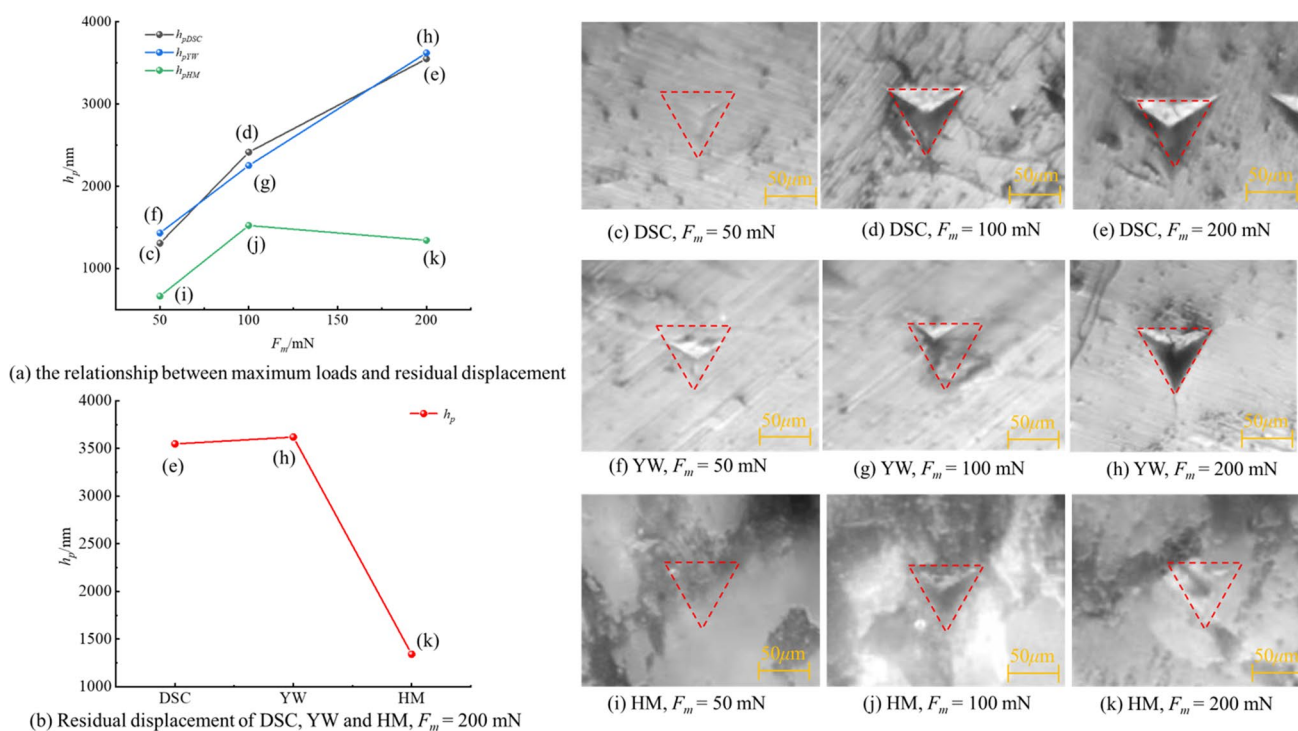


Fig. 9 The relationship between maximum loads, residual displacement and nanoindentation image

clear contour, compared to the DSC which compacts homogeneous pores and then the minerals bear load so that the indenter contour remains on the surface (Fig. 9e). Due to the excellent physical properties of HM, after large pores destruction (Fig. 9j), the hard minerals with high load-bearing capacity resist the expansion of the indenter and reduce the penetration of the indentation cracks to the surrounding area (Fig. 9k). In addition, during the unload phase, the hard minerals that have not been plastically damaged undergo elastic deformation to recover some of the displacement.

Mechanical properties at nanoscale

Elastic modulus, hardness, and fracture toughness

The elastic modulus (E_{IT}), the hardness (H_{IT}), and the fracture toughness (K_c) under different maximum loads are shown in Table 2. There are different mechanical parameters obtained at different test locations for the same maximum load. At the micro-scale, coals are typically

non-homogeneous materials with different mine components and differences in mechanical parameters. Take DSC for example, at maximum load of 100 mN, the maximum values of E_{IT} , H_{IT} , and K_c were 5.218 GPa, 0.342 GPa, and 0.191 MPa·m^{0.5}, respectively; the minimum values of E_{IT} , H_{IT} , and K_c were 3.57 GPa, 0.286 GPa, and 0.154 MPa·m^{0.5}. In addition, the elastic modulus, hardness, and fracture toughness of samples with different maximum loads are significantly different.

Elastic modulus, hardness and fracture toughness of three coals at different maximum loads using box plots (see Fig. 10).

Under different maximum loads, the distribution of the elastic modulus, hardness, and fracture toughness of DSC was concentrated according to the interquartile distance comparison. YW with increasing maximum loads, the distribution of the elastic modulus, hardness, and fracture toughness became more concentrated. HM was not only discrete but also varied over a large range with significant anisotropy.

Table 2 Elastic modulus, hardness, and fracture toughness under different maximum loads

Labels	$F_m = 50$ mN			$F_m = 100$ mN			$F_m = 200$ mN		
	E_{IT} , GPa	H_{IT} , GPa	K_c , MPa·m ^{0.5}	E_{IT} , GPa	H_{IT} , GPa	K_c , MPa·m ^{0.5}	E_{IT} , GPa	H_{IT} , GPa	K_c , MPa·m ^{0.5}
DSC-1	3.690	0.379	0.102	5.218	0.342	0.191	4.719	0.385	0.196
DSC-2	3.843	0.390	0.104	4.383	0.306	0.171	4.750	0.382	0.208
DSC-3	3.765	0.410	0.135	4.419	0.310	0.172	4.549	0.377	0.192
DSC-4	3.742	0.429	0.094	3.570	0.286	0.162	4.848	0.404	0.203
DSC-5	3.885	0.434	0.096	4.684	0.291	0.191	4.498	0.382	0.187
DSC-6	4.098	0.407	0.108	5.131	0.329	0.189	4.468	0.379	0.188
DSC-7	4.266	0.441	0.106	4.299	0.347	0.154	3.946	0.186	0.298
DSC-8	4.262	0.476	0.099	4.204	0.309	0.164	4.180	0.252	0.235
DSC-9	3.164	0.791	0.146	4.409	0.340	0.167	4.629	0.314	0.217
YW-1	4.769	0.405	0.127	4.807	0.377	0.166	4.535	0.318	0.217
YW-2	4.803	0.441	0.119	4.762	0.437	0.149	4.592	0.334	0.211
YW-3	4.442	0.358	0.129	4.771	0.394	0.160	4.605	0.337	0.211
YW-4	12.203	0.810	0.188	4.776	0.381	0.163	4.530	0.339	0.208
YW-5	8.558	0.525	0.180	4.786	0.403	0.157	5.281	0.377	0.226
YW-6	5.599	0.430	0.136	4.529	0.483	0.156	5.266	0.345	0.236
YW-7	7.971	0.387	0.206	5.164	0.472	0.152	4.857	0.390	0.201
YW-8	7.839	0.497	0.172	7.238	0.417	0.227	5.574	0.345	0.248
YW-9	4.856	0.387	0.132	18.240	0.624	0.407	5.478	0.392	0.227
HM-1	25.000	0.779	0.378	76.096	9.111	0.236	88.767	10.253	0.305
HM-2	38.220	2.251	0.250	48.826	2.762	0.448	69.988	7.943	0.297
HM-3	80.721	9.617	0.196	55.094	5.905	0.238	76.106	9.014	0.298
HM-4	28.815	1.790	0.238	30.444	0.461	0.828	55.001	3.959	0.314
HM-5	30.078	0.670	0.515	22.175	0.389	0.716	30.046	1.032	0.607
HM-6	37.049	0.660	0.621	70.857	2.941	0.488	41.422	1.979	0.488
HM-7	45.201	1.520	0.415	26.030	0.484	0.696	37.643	0.839	0.869
HM-8	37.729	1.845	0.302	36.904	0.622	0.812	37.044	0.986	0.728
HM-9	24.577	1.213	0.274	44.682	2.614	0.343	49.320	3.025	0.423

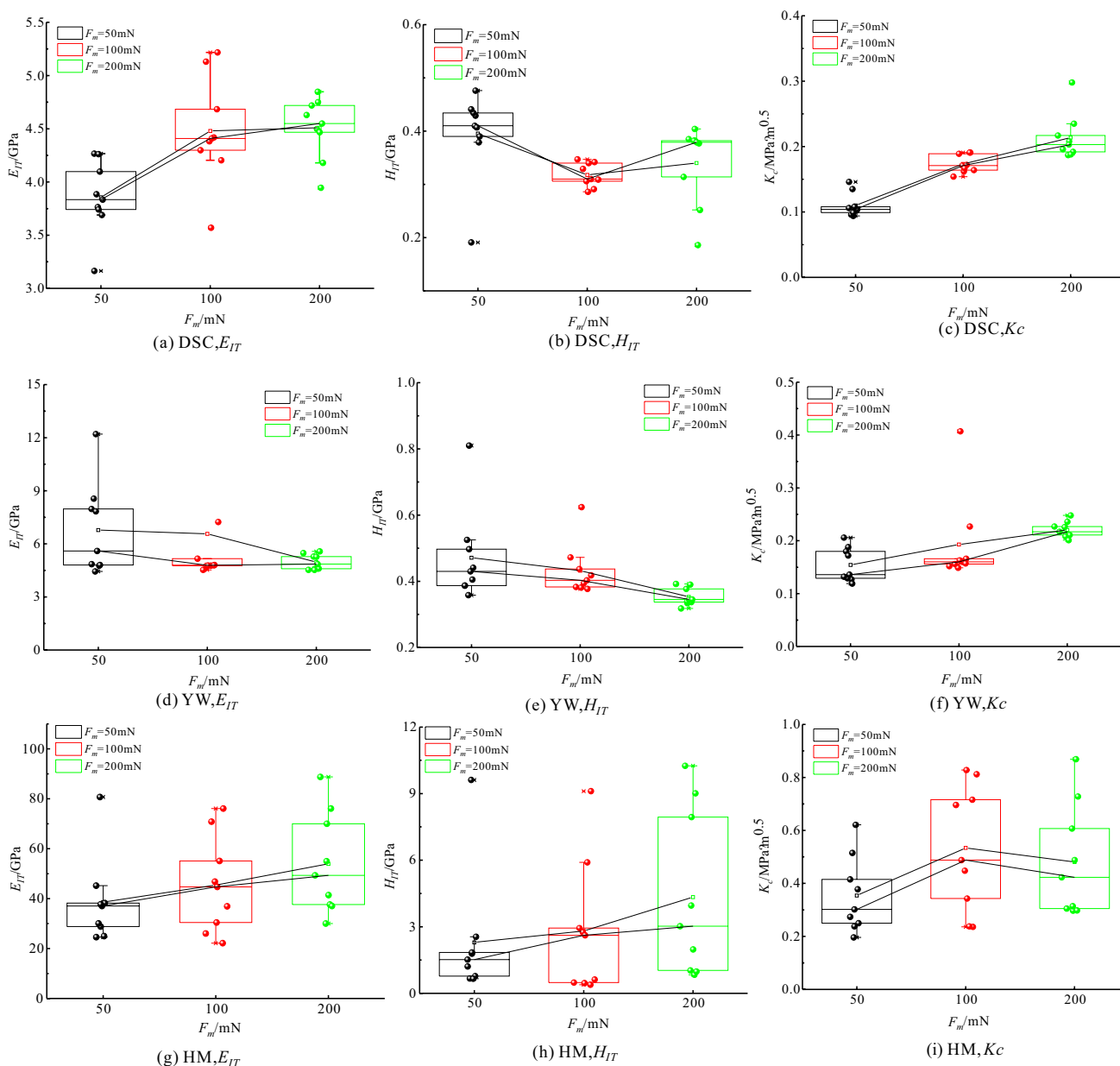


Fig. 10 Micromechanical properties under different maximum loads

Comparing DSC and YW, DSC has a more homogeneous pore structure and mineral particles, which makes its micro-mechanical parameters less discrete. YW with larger pores has a greater impact on the micro-mechanical parameter solution; then, the large pore space is gradually compressed with increasing load, the influence of pore is reduced, and only the larger particles of minerals have an impact on the results. However, the statistical results show that under high maximum load, the dispersion of the micromechanical parameters of YW is extremely small, so it indicates that the micromechanical parameters of soft coal

are mainly affected by large pores, and the influence of soft mineral particles is relatively small. The anisotropy of the micromechanical parameters of HM is overall significant, and under low maximum load, the combined effect of minerals and pore structure makes the dispersion relatively small, and with increasing maximum load, the pore is compacted. After excluding the effect of pore space, the range of variation instead increased significantly, indicating that relative to the pore structure, the physical properties of heterogeneous mineral particles have a great influence on the micromechanical parameters.

The relationship between hardness, fracture toughness, and elastic modulus

The relationship between hardness, fracture toughness, and elastic modulus under different maximum loads is obtained, and the results of the fitting are shown in Fig. 11.

From Fig. 11 a, b, and c, hardness and elastic modulus have a good linear relationship; the R^2 was 0.957, 0.913, and 0.876 for DSC, YW, and HM respectively; and the over-origin linear relationship can fit the relationship between hardness and elastic modulus well. Taking the relationship between hardness and elastic modulus of the DSC as an example, the fitted correlations R^2 were 0.984, 0.992, and 0.977 when the maximum loads are 50 mN, 100 mN, and 200 mN, respectively, further indicating that the linear relationship is independent of the maximum loads.

According to the fitting results and the fitting data (see Fig. 11 d, e, and f), the fitted correlation R^2 of DSC, YW, and HM summary were 0.93685, 0.89913, and 0.58988 respectively. The value of R^2 of fracture toughness was smaller than the R^2 of hardness because the contact projection and load information at loading is utilized in the calculation of fracture toughness, whereas the shaded area under the entire loading and unloading curve is utilized in the calculation of fracture toughness. According to Fig. 8, there are pop-in events in each coal, which cause inaccuracies in the contact projection and

loading processes. The difference in the introduced calculation parameters caused the regression relationship of the final calculation results to be inconspicuous. Taking the fracture toughness and elastic modulus relationship obtained for DSC as an example, the fitted correlation R^2 was 0.95425, 0.99618, and 0.95921 at maximum load of 50 mN, 100 mN, and 200 mN, respectively, further indicating that the linear relationship between fracture toughness and elastic modulus is independent of maximum load. However, this linear relationship for HM is unavailable, with the fitted correlation R^2 only being 0.67637, 0.56444, and 0.59564 for the maximum load equal to 50 mN, 100 mN, and 200 mN, respectively. At the same time, HM is subject to the most serious pop-in events, resulting in large errors in energy acquisition and ultimately leading to large errors in the fracture toughness results.

Influence of heterogeneous coals on macro-mechanical parameters

Comparison of micro–macro-mechanics of heterogeneous coals by multi-scale homogenization theory Mori–Tanaka method. Firstly, homogenizes the solid phase of coal matrix and the porosity into a coal matrix-porous medium, and then the coal matrix-porous medium and the mineral phase into a homogeneous material equivalent to the actual coal (Li

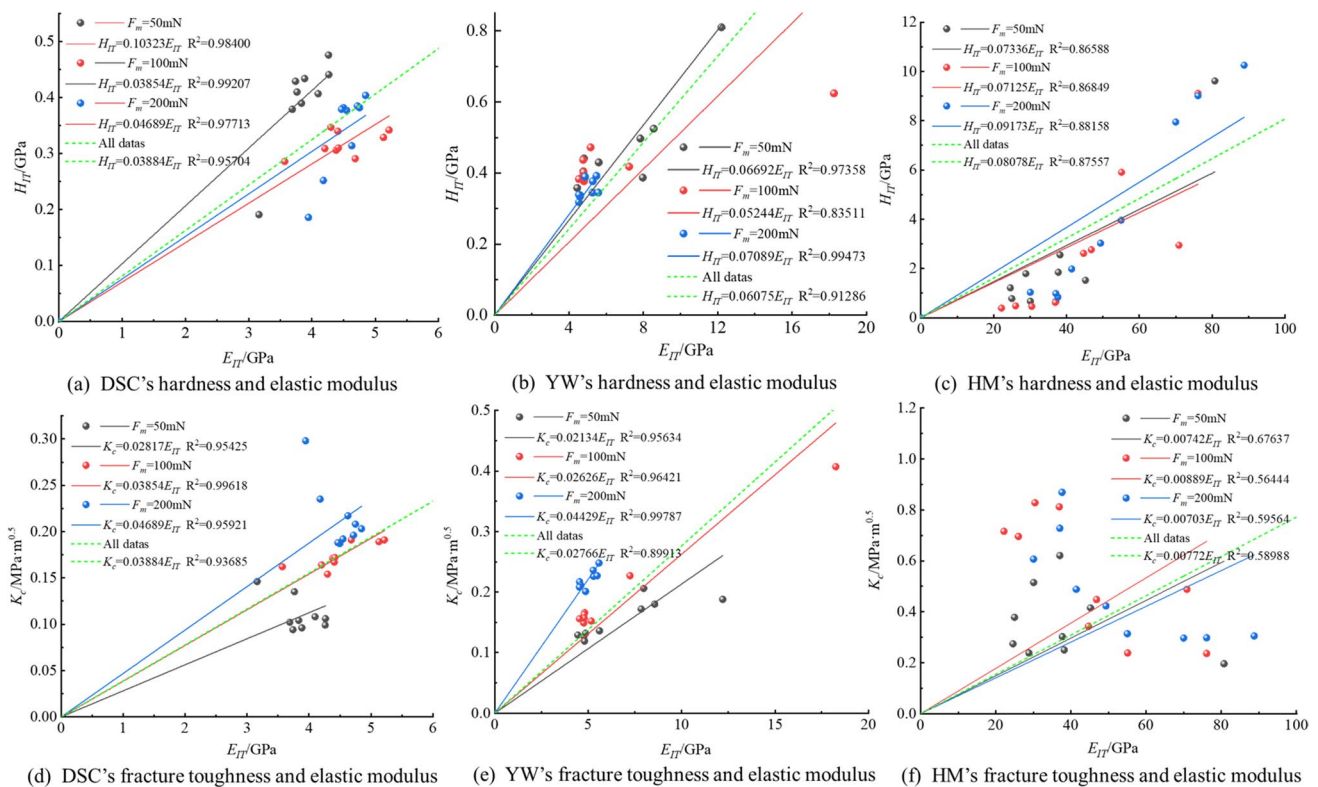


Fig. 11 Relation and fitting curve of hardness, fracture toughness and elastic modulus

et al. 2022a, b, c, d; Meng et al. 2023). The homogenization process is shown in Fig. 12.

Following the homogenization process, the analysis starts with the second step of the homogenization process, which is calculated as follows:

$$K^{\text{hom}} = \frac{\sum \frac{f_r k_r}{3k_r + 4\mu_0}}{\sum \frac{f_r}{3k_r + 4\mu_0}} \tag{13}$$

$$G^{\text{hom}} = \frac{\sum \frac{f_r \mu_r}{\mu_0(9k_0 + 8\mu_0) + 6\mu_r(k_0 + 2\mu_0)}}{\sum \frac{f_r}{\mu_0(9k_0 + 8\mu_0) + 6\mu_r(k_0 + 2\mu_0)}} \tag{14}$$

where f_0 is the volume fraction of coal matrix, f_1 is the volume fraction of clay minerals, f_2 is the volume fraction of quartz minerals, and f_3 is the volume fraction of carbonate minerals.

The elasticity modulus of the coal matrix of each coal during the homogenization analysis can be approximated as the average modulus of elasticity at a maximum load of 200 mN. Their bulk modulus k and shear modulus μ are obtained from the following equation:

$$k_r = \frac{E}{3(1 - 2\nu)} \tag{15}$$

$$\mu_r = \frac{E}{2(1 + \nu)} \tag{16}$$

where E is the modulus of each phase and ν is the Poisson's ratio of each phase.

Based on the existing research results (Abou-Chakra Guéry et al. 2010; Huang et al. 2014; Zeng et al. 2019), the elasticity modulus and Poisson's ratio of clay minerals are selected as 20 GPa, 0.35; quartz minerals as 90 GPa, 0.15; carbonate minerals as 85 GPa, 0.25. The first step of the homogenization process is to homogenize the solid phase of the coal matrix and its pores, so the mechanical parameters of coal matrix obtained by homogenization will also be determined by the two, and the bulk modulus and shear modulus of coal matrix will be determined by both, and shear modulus are calculated as follows:

$$k_0 = \frac{4(1 - \varphi)k_c \mu_c}{4\mu_c + 3\varphi k_c} \tag{17}$$

$$\mu_0 = \frac{(1 - \varphi)\mu_c}{1 + 6\varphi \frac{k_c + 2\mu_c}{9k_c + 8\mu_c}} \tag{18}$$

where φ is the porosity of the coal sample obtained by the small angle X experiment, k_c is the bulk modulus of the solid phase of the coal matrix, and μ_c is the shear modulus of the solid phase of the coal matrix.

The homogenized elasticity modulus E^{hom} can be obtained by the following equations respectively.

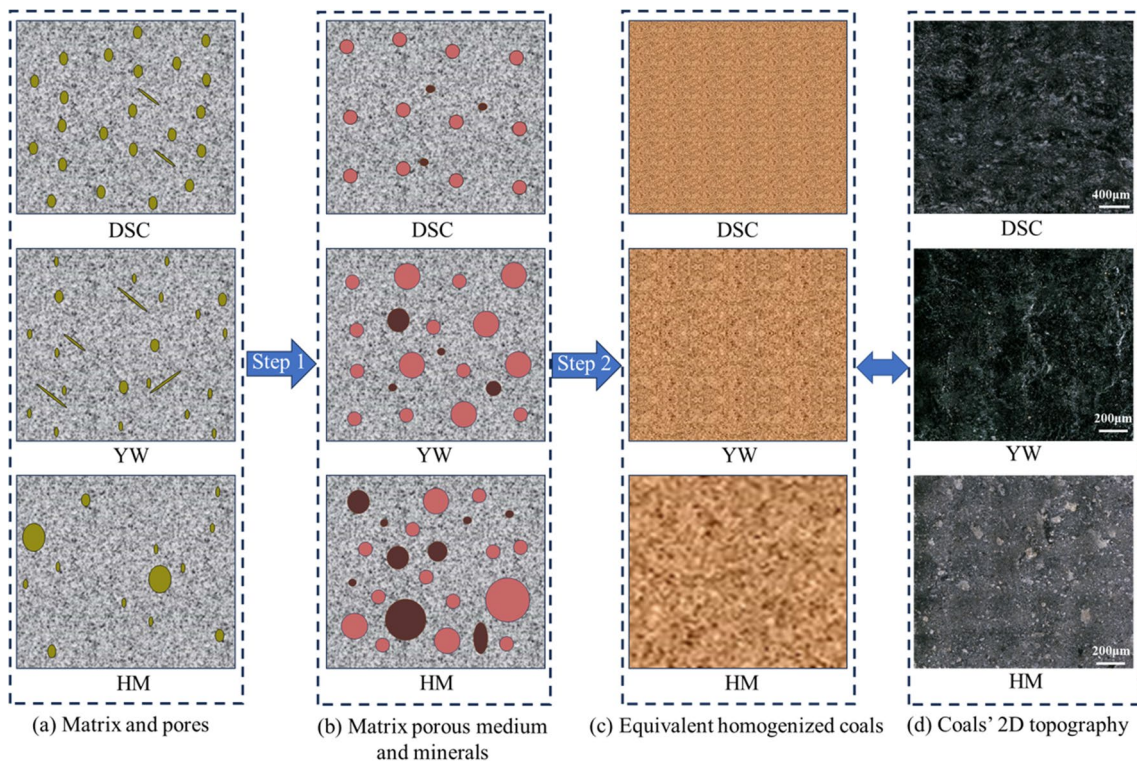


Fig. 12 Schematic diagram of homogenization process

$$E^{\text{hom}} = \frac{9K^{\text{hom}}G^{\text{hom}}}{3K^{\text{hom}} + G^{\text{hom}}} \quad (19)$$

Figure 13 shows a comparison between the microscopic elastic modulus measured by nanoindentation experiments for three samples and the equivalent macroscopic elastic modulus results obtained after homogenization of three samples.

The two elastic modulus results are similar, and the microscopic modulus is larger than the corresponding macroscopic modulus, which indicates that the microscopic mechanical properties derived from nanoindentation tests are good guides to the macroscopic rock mechanical properties, but with the increase of scale, the minerals and pores contained in the coal increase in the degree of heterogeneity, the structure is more complex, and the deterioration of the coal by the pores or primary cleavage is more pronounced; thus, the micro-modulus is generally larger than the macro-modulus. The deviation rates of the two elastic moduli of DSC, YW and HM, are 15.588, 14.651, and 13.836, respectively, showing a decreasing trend. YW has a higher degree of non-homogenization than DSC, and contains a more complex structure, which is closer to the characteristics of the large-scale specimen, so the deviation rate is lower. HM, in addition to the above reasons, is also due to the fact that it contains a large number intact of hard minerals, the minerals have significant elastic properties and are not prone to plastic deformation, and as the scale is upgraded, the plastic deformation has less effect on the elastic modulus; thus, the deviation rate of HM is the smallest.

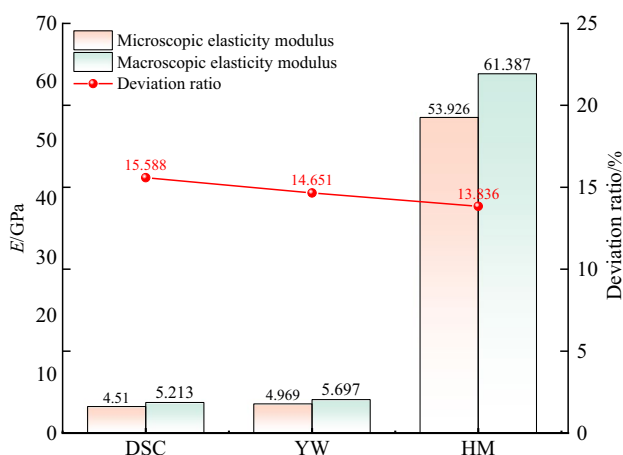


Fig. 13 Elastic modulus of microscopic and macroscopic

Conclusions

Nanoindentation is an efficient and non-destructive mechanical testing method widely used in the micromechanical property testing of metals, rocks, and various materials. This paper applied nanoindentation, XRD, SAXS, a high magnification microscope, and mechanical parameter scale-up to investigate the nanomechanical properties of three heterogeneous coals being dominant by component and pores. The main conclusions are drawn as follows:

- (1) DSC, YW, and HM have significant heterogeneity in mineral characteristics as well as pore structure. DSC has the loosest structure with uniformly spread pores, good uniformity of its aperture, fewer cracks, and weak physical properties of small mineral particles; YW has a more compact structure with significant cracks, and weak physical properties of more uniform size and distribution of mineral particles; HM has the most compact structure but has significant large pore structure and non-uniformly distributed strength of hard minerals in large particles.
- (2) Pop-in events appear in the curves of different coals, with maximum load and heterogeneity affecting the frequency of pop-in events. DSC appears once at a maximum load of 50 mN due to the destruction of the uniformly distributed large pore, once at a maximum load of 100 mN due to the pore pressure breaking through with the surrounding fracture, and once at a maximum load of 200 mN due to the soft minerals. YW has no pop-in event at the maximum load of 50 mN due to the heterogeneous pore structure, and the pop-in event does not occur due to the destruction of the soft small pore by the low load, and the pop-in event occurs once at 100mN when the large pore suddenly begins to destroy itself. YW has three pop-in events at a maximum load of 200 mN and the curves have the characteristics of a pop-in event and many displacements of sudden progress. It is characterized by alternating destruction of soft minerals and macropores, and failure of soft minerals or destruction of macropores affects the time of the pop-in event. HM at a maximum load of 50 mN, pop-in event occurred four times due to its strong mechanical properties. High loads cause a large number of large pores and small pores to be destroyed, resulting in multiple pop-in events, HM at maximum load of 100 mn, pop-in event appeared twice, which was formed by the combined formation of pores and a small amount of soft minerals. HM at a maximum load of 200 mN, pop-in event occurs twice and is produced by the destruction of soft minerals and slippage of some hard minerals.

- (3) For coal containing soft minerals, the heterogeneity of its pore structure has little effect on the residual displacement, while the residual displacement of coal with hard minerals is much smaller than that of coal with soft minerals. With the increase of the maximum load, the residual displacement has a tendency to increase. The different distribution of heterogeneous pores will cause, the anisotropy of the residual displacement, and the resistance of hard minerals to the indenter will recover part of the deformation and reduce the residual displacement with the increase of the maximum load and increase in the law. The greater the heterogeneity of the coal, the greater the dispersion of the mechanical parameters. The micromechanical parameters of soft coal are mainly affected by large pores, and the size degree of mineral particles has less influence on them, while the micromechanical parameters of hard coal are mainly affected by mineral particles. Further analysis shows that hardness and modulus of elasticity have a good linear relationship, and neither the maximum load nor the heterogeneity of the coal affects them, and fracture toughness and modulus of elasticity have a certain linear relationship. Not only that, but the more significant pop-in event weakened its linear relationship more obviously.
- (4) The microscopic results of heterogeneous coal measured by nanoindentation approximate the macroscopic mechanical parameters, and the deviation rate is below 15.588%, but the simplifying effect of the microscopic experiments on the macroscopic coal components and structure makes the microscopic modulus large. When the coal heterogeneity is greater, the closer the macro-coal characteristics are, the results of the accuracy are higher. Not only that, but when the coal's hard mineral content is greater, its high elasticity will also increase the accuracy of the macro mechanical parameters.

Author contribution Baisheng Nie proposed the topic. Hengyi He wrote the manuscript. Peng Liu carried out the visualization and paper editing. Xianfeng Liu carried out visualization. Bozhi Deng carried out the review analysis. Yulong Zhao edited the manuscript. Hao Zhang contributed to the interpretation of the results. Mingwei Cao edited the manuscript.

Funding This work was supported by the National Natural Science Foundation of China (52204206, 52274173) and the Open Fund Project Funded by State Key Laboratory of Mining Response and Disaster Prevention and Control in Deep Coal Mines (Grant No. SKLMRDPC21KF12).

Data availability Please contact the corresponding author for data requests.

Declarations

Ethics approval Not applicable.

Consent to participate Not applicable.

Consent for publication Not applicable.

Competing interests The authors declare no competing interests.

References

- Abou-Chakra Guéry A, Cormery F, Shao JF, Kondo D (2010) A comparative micromechanical analysis of the effective properties of a geomaterial: effect of mineralogical compositions. *Comput Geotech* 37:585–593. <https://doi.org/10.1016/j.compgeo.2010.02.008>
- Bhuiyan MAH, Bodrud-Doza M, Rakib MA, Saha BB, Islam SMD (2021) Appraisal of pollution scenario, sources and public health risk of harmful metals in mine water of Barapukuria coal mine industry in Bangladesh. *Environ Sci Pollut Res Int* 28:22105–22122. <https://doi.org/10.1007/s11356-020-11999-z>
- Borodich FM, Bull SJ, Epshtein SA (2015) Nanoindentation in studying mechanical properties of heterogeneous materials. *J Min Sci* 51:470–476. <https://doi.org/10.1134/S1062739115030072>
- Cao D, Li X, Zhang S (2007) Influence of tectonic stress on coalification: stress degradation mechanism and stress polycondensation mechanism. *Sci China, Ser D Earth Sci* 50:43–54. <https://doi.org/10.1007/s11430-007-2023-3>
- Cao Q, Yan R, Yang L, Takaoka M (2023) Effects of water–coal interactions on coal mine water quality in China: a lixiviation experiment and actual water quality investigation. *Environ Sci Pollut Res Int* 30:107350–107364. <https://doi.org/10.1007/s11356-022-25116-9>
- Chao J, Chu T, Yu M et al (2021) An experimental study on the oxidation kinetics characterization of broken coal under stress loading. *Fuel* 287:119515. <https://doi.org/10.1016/j.fuel.2020.119515>
- Cheng Y, Pan Z (2020) Reservoir properties of Chinese tectonic coal: a review. *Fuel* 260:116350. <https://doi.org/10.1016/j.fuel.2019.116350>
- Epshtein SA, Borodich FM, Bull SJ (2015) Evaluation of elastic modulus and hardness of highly inhomogeneous materials by nanoindentation. *Applied Physics. A, Mater Sci Proc* 119:325–335. <https://doi.org/10.1007/s00339-014-8971-5>
- Feng H, Zhou J, Chai B et al (2020) Groundwater environmental risk assessment of abandoned coal mine in each phase of the mine life cycle: a case study of Hongshan coal mine, North China. *Environ Sci Pollut Res Int* 27:42001–42021. <https://doi.org/10.1007/s11356-020-10056-z>
- Hu Z, Lynne K, Delfanian F (2015) Characterization of materials' elasticity and yield strength through micro-/nano-indentation testing with a cylindrical flat-tip indenter. *J Mater Res* 30:578–591. <https://doi.org/10.1557/jmr.2015.4>
- Huang Y, Shen WQ, Shao JF, Abou-Chakra Guéry A, Jia Y (2014) Multi-scale modeling of time-dependent behavior of claystones with a viscoplastic compressible porous matrix. *Mech Mater* 79:25–34. <https://doi.org/10.1016/j.mechmat.2014.08.003>
- Karacan C, Ruiz F, Cotè M, Phipps S (2011) Coal mine methane: a review of capture and utilization practices with benefits to mining safety and to greenhouse gas reduction. *Int J Coal Geol* 86:121–156. <https://doi.org/10.1016/j.coal.2011.02.009>
- Kossovich EL, Borodich FM, Epshtein SA, Galanov BA, Minin MG, Prošina VA (2019) Mechanical, structural and scaling properties of coals: depth-sensing indentation studies. *Applied Physics. A,*

- Materials Science & Processing 125:1–15. <https://doi.org/10.1007/s00339-018-2282-1>
- Kossovich E, Borodich F, Epshtein S, Galanov B, Minin M, Prošina V (2019) Mechanical, structural and scaling properties of coals: depth-sensing indentation studies. *Applied Physics A* 125. <https://doi.org/10.1007/s00339-018-2282-1>
- Kossovich E, Epshtein S, Krasilova V, Hao J, Minin M (2023) Effects of coals microscale structural features on their mechanical properties, propensity to crushing and fine dust formation. *Int J Coal Sci Technol* 10. <https://doi.org/10.1007/s40789-023-00578-5>
- Le T, Oh J (2022) Longwall face stability analysis from a discontinuum-discrete fracture network modelling. *Tunn Undergr Space Technol* 124:104480. <https://doi.org/10.1016/j.tust.2022.104480>
- Li W, Jiang B, Gu S (2022) Effect of water on mechanical properties of coal measures mudstone using nanoindentation. *Geofluids* 2022:1–16. <https://doi.org/10.1155/2022/9032572>
- Li Y, Chen J, Elsworth D, Pan Z, Ma X (2022) Nanoscale mechanical property variations concerning mineral composition and contact of marine shale. *Geosci Front* 13:101405. <https://doi.org/10.1016/j.gsf.2022.101405>
- Li Y, Chen J, Yang J, Liu J, Tong W (2022) Determination of shale macroscale modulus based on microscale measurement: a case study concerning multiscale mechanical characteristics. *Pet Sci* 19:1262–1275. <https://doi.org/10.1016/j.petsci.2021.10.004>
- Li Y, Pan S, Ning S, Shao L, Jing Z, Wang Z (2022) Coal measure metallogeny: metallogenic system and implication for resource and environment. *Sci China Earth Sci* 65:1211–1228. <https://doi.org/10.1007/s11430-021-9920-4>
- Li G, Li Z, Du F, Cao Z (2023) Mechanical mechanism of rib spalling and sensitivity analysis of gangue parameters to rib spalling in gangue-bearing coal seams. *Environ Sci Pollut Res Int* 30:38713–38727. <https://doi.org/10.1007/s11356-022-25033-x>
- Li L, Khraishi T, Shen Y (2023) Investigation of the effect of indentation spacing, edge distance and specimen thickness on the measurement of hardness. *J Mech Sci Technol* 37:687–696. <https://doi.org/10.1007/s12206-023-0112-7>
- Liu X, Wang L, Kong X et al (2022) Role of pore irregularity in methane desorption capacity of coking coal. *Fuel* 314:123037. <https://doi.org/10.1016/j.fuel.2021.123037>
- Liu Y, Yang C, Wang J, Xiong Y, Peng P (2023) Rheology of coal at particle level characterized by nanoindentation. *Nat Resour Res* 32:1359–1380. <https://doi.org/10.1007/s11053-023-10188-2>
- Ma Z, Pathegama Gamage R, Zhang C (2020) Application of nanoindentation technology in rocks: a review. *Geomech Geophys Geo Energy Ge Resour* 6. <https://doi.org/10.1007/s40948-020-00178-6>
- Manjunath G, Jha B (2019) Nanoscale fracture mechanics of gondwana coal. *Int J Coal Geol* 204:102–112. <https://doi.org/10.1016/j.coal.2019.02.007>
- Meng J, Lyu C, Wang J et al (2023) Mechanical properties and failure mechanisms of different rank coals at the nanoscale. *Fuel* 345:128209. <https://doi.org/10.1016/j.fuel.2023.128209>
- Miller M, Bobko C, Vandamme M, Ulm F (2008) Surface roughness criteria for cement paste nanoindentation. *Cem Concr Res* 38:467–476. <https://doi.org/10.1016/j.cemconres.2007.11.014>
- Oliver W, Pharr G (1992) An improved technique for determining hardness and elastic modulus using load and displacement sensing indentation experiments. *J Mater Res* 7:1564–1583. <https://doi.org/10.1557/JMR.1992.1564>
- Ou X, Ouyang L, Xu X, Wang L (2022) Case study on floor heave failure of highway tunnels in gently inclined coal seam. *Eng Fail Anal* 136:106224. <https://doi.org/10.1016/j.engfailanal.2022.106224>
- Phani P, Hackett B, Walker C, Oliver W, Pharr G (2023) High strain rate nanoindentation testing: recent advancements, challenges and opportunities. *Curr Opin Solid State Mater Sci* 27:101054. <https://doi.org/10.1016/j.cossms.2022.101054>
- Qin B, Shi Z, Hao J, Ye D, Liang B, Sun W (2022) Analysis of the space–time synergy of coal and gas co-mining. *ACS Omega* 7:13737–13749. <https://doi.org/10.1021/acscomega.2c00034>
- Róžański A, Róžańska A, Sobótka M, Pachnicz M, Bukowska M (2021) Identification of changes in mechanical properties of sandstone subjected to high temperature: meso- and micro-scale testing and analysis. *Arch Civ Mech Eng* 21. <https://doi.org/10.1007/s43452-021-00187-6>
- Shi X, Jiang S, Wang Z, Bai B, Xiao D, Tang M (2020) Application of nanoindentation technology for characterizing the mechanical properties of shale before and after supercritical CO₂ fluid treatment. *J Co2 Util* 37:158–172. <https://doi.org/10.1016/j.jcou.2019.11.022>
- Song B, Zhai X, Ma T, Wang B, Hao L, Zhou Y (2023) Effect of water immersion on pore structure of bituminous coal with different metamorphic degrees. *Energy* 274:127449. <https://doi.org/10.1016/j.energy.2023.127449>
- Sun C, Li G, Zhang S, Xu J, Yang H (2020) Mechanical and heterogeneous properties of coal and rock quantified and mapped at the microscale. *Appl Sci* 10:342. <https://doi.org/10.3390/app10010342>
- Tu Q, Cheng Y, Ting R, Wang Z, Jia L, Lei Y (2019) Role of tectonic coal in coal and gas outburst behavior during coal mining. *Rock Mech Rock Eng* 52:4619–4635. <https://doi.org/10.1007/s00603-019-01846-0>
- Wang Z, Cheng Y, Wang L, Wang C, Lei Y, Jiang Z (2020) Analysis of pulverized tectonic coal gas expansion energy in underground mines and its influence on the environment. *Environ Sci Pollut Res Int* 27:1508–1520. <https://doi.org/10.1007/s11356-019-06757-9>
- Wang S, Li X, Qin Q (2022) Study on surrounding rock control and support stability of ultra-large height mining face. *Energies* 15:6811. <https://doi.org/10.3390/en15186811>
- Xu J, Tang X, Wang Z, Feng Y, Bian K (2020) Investigating the softening of weak interlayers during landslides using nanoindentation experiments and simulations. *Eng Geol* 277:105801. <https://doi.org/10.1016/j.enggeo.2020.105801>
- Xue Y, Liu J, Ranjith P, Gao F, Xie H, Wang J (2022) Changes in microstructure and mechanical properties of low-permeability coal induced by pulsating nitrogen fatigue fracturing tests. *Rock Mech Rock Eng* 55:7469–7488. <https://doi.org/10.1007/s00603-022-03031-2>
- Yang L, Xu J, Fang J, Cao Z, Li T, Song H (2020) Risk evaluation of groundwater leakage in coal seam goaf: a case study in the Lingxin mining area. *Environ Sci Pollut Res Int* 27:26066–26078. <https://doi.org/10.1007/s11356-020-08995-8>
- Yu H, Zhang Y, Lebedev M et al (2018) Nanoscale geomechanical properties of western Australian coal. *J Pet Sci Eng* 162:736–746. <https://doi.org/10.1016/j.petrol.2017.11.001>
- Zeng Q, Wu Y, Liu Y, Zhang G (2019) Determining the micro-fracture properties of Antrim gas shale by an improved micro-indentation method. *J Nat Gas Sci Eng* 62:224–235. <https://doi.org/10.1016/j.jngse.2018.12.013>
- Zhang X, Li X, Gao X (2016) Hydrochemistry and coal mining activity induced karst water quality degradation in the Niangziguan karst water system, China. *Environ Sci Pollut Res Int* 23:6286–6299. <https://doi.org/10.1007/s11356-015-5838-z>
- Zhang Y, Lebedev M, Al-Yaseri A et al (2018) Nanoscale rock mechanical property changes in heterogeneous coal after water adsorption. *Fuel* 218:23–32. <https://doi.org/10.1016/j.fuel.2018.01.006>
- Zhang G, Ranjith P, Lyu Q (2022) Direct evidence of CO₂ softening effects on coal using nanoindentation. *Energy* 254:124221. <https://doi.org/10.1016/j.energy.2022.124221>
- Zhang S, Sun L, Qin B, Wang H, Qi G (2022) Characteristics and main factors of foam flow in broken rock mass in coal mine goaf. *Environ Sci Pollut Res Int* 29:47095–47108. <https://doi.org/10.1007/s11356-022-19208-9>

- Zhao J, Huang P, Xu KW, Wang F, Lu TJ (2018) Indentation size and loading strain rate dependent creep deformation of nanocrystalline mo. *Thin Solid Films* 653:365–370. <https://doi.org/10.1016/j.tsf.2018.03.068>
- Zhong S, Lin D (2022) Evaluation of the coordination degree of coal and gas co-mining system based on system dynamics. *Sustainability* 14:16434. <https://doi.org/10.3390/su142416434>
- Zhu Y, Li C, Li L, Yang K, Yang Y, Zhang G (2023) Dynamic assessment and system dynamics simulation of safety risk in whole life cycle of coal mine. *Environ Sci Pollut Res Int* 30:64154–64167. <https://doi.org/10.1007/s11356-023-26958-7>

Publisher's Note Springer Nature remains neutral with regard to jurisdictional claims in published maps and institutional affiliations.

Springer Nature or its licensor (e.g. a society or other partner) holds exclusive rights to this article under a publishing agreement with the author(s) or other rightsholder(s); author self-archiving of the accepted manuscript version of this article is solely governed by the terms of such publishing agreement and applicable law.